CrystEngComm

Accepted Manuscript

This article can be cited before page numbers have been issued, to do this please use: L. Zhu, T. Zheng, J. Zheng, N. Zhang, C. yu, Q. Liao, Q. Shu and B. H. Chen, *CrystEngComm*, 2017, DOI: 10.1039/C7CE00702G.

View Article Online
DOI: 10.1039/C7CE00702G

Journal Name

ARTICLE

Synthesis of Ru/CoNi crystals with different morphologies for catalytic hydrogenation

Received 00th January 20xx,
Accepted 00th January 20xx

DOI: 10.1039/x0xx00000x

www.rsc.org/

Lihua Zhu,[*ab] Tuo Zheng,[a] Jinbao Zheng,[b] Changlin Yu,[a] Nuowei Zhang,[b] Qi Liao,[a] Qing Shu[a] and Bing H Chen[*b]

Cobalt-nickel alloy crystals with different morphologies, such as flower-like, column-like, mushroom-like and dendrite-like, were prepared by a facile hydrothermal or solvothermal reduction approach without the addition of any surfactant, using hydrazine hydrate as reducing agent, ethanediamine as capping agent and the mixture of nickel(II) chloride hexahydrate ($NiCl_2·6H_2O$) and cobalt(II) chloride hexahydrate ($CoCl_2·6H_2O$) as precursor. The effect of hydrothermal temperature (120, 150 or 180 °C) and solvent (water or ethanol) on the shape of the CoNi crystal was investigated in this work. The corresponding Ru/CoNi catalysts (Ru-on-CoNi nanocrystal) were obtained via galvanic replacement reaction. The size, element chemical state, morphologies and structures of the CoNi and Ru/CoNi samples were characterized by X-ray diffraction (XRD), scanning electronic microscopy (SEM), energy dispersive X-ray spectroscopy (EDS), X-ray photoelectron spectroscopy (XPS), high-sensitivity low-energy ion scattering (HS-LEIS) techniques. The catalytic performance of the as-synthesized catalysts was evaluated by using benzene hydrogenation reaction. And the Ru/CoNi catalyst with dendrite-like morphology exhibited the highest catalytic hydrogenation activity among the Ru/CoNi catalysts with different shapes. It was mainly due to its high Ru dispersion, many defect sites and positive synergistic effect among ruthenium, nickel and cobalt related species. Importantly, the cost of recycling the Ru/CoNi catalysts was relatively low because they could be recycled by magnetic separation.

1 Introduction

Generally, multi-metallic (such as bimetallic or tri-metallic) nanomaterials take on more excellent properties (e.g. catalytic performance) than the corresponding mono-metallic nanomaterials, and the multi-metallic nanomaterials even show unique behavior.[1-5] Their properties are quite dependent on the morphologies, size, composition and structures of the nanomaterials.[6-8] The size, morphology, element chemical state, composition and nanostructure of the bimetallic nanocatalyst play an important role in determining its selectivity, activity and stability.[6-8] Hence, the controlled synthesis of the multi-metallic nanocatalysts has attracted more and more interests from chemists and material scientists.[9]

Cobalt-nickel bimetallic nanomaterials are extensively applied in the fields of memory storage, magnetic recording and magnetic resonance imaging, biomedical, microwave absorbers, microelectromechanical systems and catalysis.[10-17] So it is of significance to prepare high-quality cobalt-nickel nanomaterials or micro-particles. Currently, some approaches have been applied to obtain CoNi nanomaterials with different morphologies, such as liquid chemical reduction and hydrothermal synthesis. The reported shapes of the CoNi crystal mainly consist of CoNi alloy particles,[18] Ni@Co core-shell,[19] CoNi nanowires,[20,21] CoNi nanofibers,[22] rose-like NiCo nanoflowers,[23] chain-like CoNi crystal,[24,25] CoNi nanourchins, nanowires and hollow microspheres,[20] CoNi nanorings,[26] CoNi nanoneedles,[27] CoNi films,[13] CoNi nanodumbbells,[28] handkerchief-like NiCo nanostructures,[29] rod-like, wheat-like and leaf-like CoNi structures.[30] For instance, Li *et al.* prepared the leaf-like CoNi nanomaterial at 180 °C via wet-chemical reduction method without adding any surfactant or template, using sodium citrate as complexing agent. They also investigated the effect of synthesis temperature on the morphology of the products, and found that low temperature was favorable to form CoNi microspheres.[30] CoNi nanourchins and nanowires were obtained by using microwave-assisted polyol-synthesis method in Shen' group.[20] And it was found that the catalytic activity and selectivity of the CoNi catalyst in glycerol hydrogenolysis reaction were strongly affected by its shape and size. Cobalt-nickel alloy flower-like superstructures were synthesized at 150 °C via a simple hydrothermal reduction method with the addition of potassium sodium tartrate.[31] However, to the best of our knowledge, the synthesis of mushroom-like and dendrite-like CoNi crystal and the effect of solvent on the shape of CoNi were hardly reported. In our

---

[a] *School of Metallurgy and Chemical Engineering, Jiangxi University of Science and Technology, Ganzhou 341000, Jiang Xi, China. E-mail: lihuazhu@stu.xmu.edu.cn. Fax: +86-797-8312204.*

[b] *Department of Chemical and Biochemical Engineering, National Engineering Laboratory for Green Productions of Alcohols-Ethers-Esters, College of Chemistry and Chemical Engineering, Xiamen University, Xiamen 361005, China. E-mail: chenbh@xmu.edu.cn; Fax: (+) 86-592-2184822; Tel: +86-592-2185253.*

View Article Online
DOI: 10.1039/C7CE00702G

study, focusing on the above two topics, the CoNi integral structure with different morphologies (such as flower-like, column-like, mushroom-like and dendrite-like) were acquired by adjusting the synthesis temperature and solvent.

For aromatics hydrogenation reactions, the Ni-based,[32] Pt-based,[33] Ru-based,[34,35] Pd-based,[36] Rh-based,[37] Ir-based[38] and multi-metallic nanocatalysts[39] were widely used, and with excellent catalytic performance. But these catalysts were of high recycling cost due to their nanoscale. In addition, much heat was generated in arene hydrogenation reactions and needed to be removed. To solve the above two problems, the CoNi alloy crystal with excellent magnetic property, outstanding heat-conducting property and monolith were designed and prepared, and it was used as the catalyst support for depositing ruthenium. Herein, the CoNi alloy samples were synthesized by a simple hydrothermal or solvothermal method. And the morphologies of CoNi were successfully controlled by varying the synthesis temperature or solvent. A proposed growth mechanism of various morphologies of CoNi alloy crystal was also provided. The Ru/CoNi catalysts were gained by galvanic replacement reaction. Benzene hydrogenation was used as a model reaction, in which the catalytic performance of the Ru/CoNi catalysts with different shapes was evaluated. The reasons for the difference in their catalytic activity were also investigated.

2 Experimental

The chemicals with analytic grade were purchased from Sinopharm Chemical Reagent Co. Ltd. (Shanghai, China). They were used as received. Deionized water was prepared in our group by using Milli-Q system.

The CoNi samples were prepared through the following steps. $NiCl_2 \cdot 6H_2O$ (0.6500 g) and $CoCl_2 \cdot 6H_2O$ (0.6500 g) were dissolved in deionized water (30 mL), forming the aqueous mixture of $NiCl_2$ and $CoCl_2$ solution. 5 mL of anhydrous ethanol was added to the above solution under magnetic stirring for 10 min, followed by the addition of anhydrous ethanediamine (EDA-5 mL). The aqueous NaOH solution (5 mL) (1.8130 g NaOH dissolved in 5 mL deionized water) was added into the above-obtained solution with agitation for 10 min. Then the addition of reducing agent (85 wt% hydrazine hydrate-$N_2H_4 \cdot H_2O$) (5 mL) was performed. After stirring for 10 min, the mixture liquid was transferred into a 100 mL Teflon-lined stainless-steel autoclave and sealed. The hydrothermal synthesis process was maintained at X °C for 1 h; where X = 120, 150 or 180 °C. After the reaction completed, the autoclave was naturally cooled down to room temperature (RT). The solid product was washed thoroughly with deionized water and anhydrous ethanol, and then dried in vacuum at 60 °C for 6 h, the as-obtained CoNi samples were denoted as CoNi-X, where X represented the synthesis temperature (120, 150 or 180 °C). With the purpose of investigating the effect of solvent on the morphology of CoNi nanostructures, the mixture of $NiCl_2 \cdot 6H_2O$ (0.6500 g) and $CoCl_2 \cdot 6H_2O$ (0.6500 g) were dissolved in 30 mL of ethanol instead of deionized water, forming the ethanol mixture of $NiCl_2$ and $CoCl_2$ solution. And other experimental conditions were unchanged (synthesis temperature-120 °C and reaction time-1 h). The obtained CoNi sample was signed as CoNi-120-ethanol.

The Ru/CoNi tri-metallic catalysts (Ruthenium loaded on the CoNi crystal) were obtained by the galvanic replacement reaction method.[40-45] The main steps were described below. 0.1 g of the as-prepared CoNi crystal was dispersed in a certain amount of $RuCl_3$ aqueous solution (9.64×10^{-3} mol L^{-1}), ultrasound-assisted synthesis at RT for 2 h. The Ru/CoNi catalysts were collected by filtration, repeatedly washed with deionized water and anhydrous ethanol, and then dried in a vacuum oven at 60 °C for 6 h. The Ru content in the catalysts was analyzed by energy dispersive X-ray spectroscopy (EDS). The Ru loading is 1.10 wt% in the Ru/CoNi catalysts, very consistent with the results obtained from inductively coupled plasma atomic mass spectrometry (ICP-MS) tests.

Characterizations for the samples: Powder X-ray diffraction (XRD) patterns for the samples were recorded on a Rigaku Ultima IV X-ray diffractometer equipped with high-speed array detection system. Cu *Ka* radiation was used as the X-ray source, operating at 40 kV and 30 mA. The 2θ scanning range was 10°~90°. The scanning electron microscope (SEM) and EDS analysis of the samples were conducted on a field-emission scanning electron microscope (MLA650F). XPS measurements for the catalysts were run on PHI Quantum 2000 Scanning ESCA Microprobe with monochromatic Al *Ka* radiation (1486.6 eV). The high-sensitivity low-energy ion scattering (HS-LEIS) tests for the catalysts were performed on IonTOF Qtac100 low-energy ion scattering analyzer, to gain the atomic composition of outer surface of the catalysts. $^{4}He^{+}$ ions with a kinetic energy of 3 keV were applied at a low ion flux equal to 1325 pA cm^{-2}. $^{20}Ne^{+}$ ions with a kinetic energy of 5 keV were applied at a low ion flux of 1600 pA cm^{-2}. The scattering angle was 145°.

Catalytic measurements of the hydrogenation of benzene were carried out in a stainless steel autoclave (Parr 4848). Catalyst-0.0500 g and benzene-10 mL were mixed evenly, and then taken into the reactor. The closed reactor was firstly purged with hydrogen for 1 min to remove air, and then H_2 was continuously added into the reactor until the initial pressure increased to 4.8 MPa. The reagents were quickly heated to the desired reaction temperature (100 °C), and maintained for 1 h under vigorous stirring (500 rpm). After the reaction was over, the reaction system was stopped and quickly cooled down to RT. Quantitative analysis of the products were conducted with a gas chromatography (Shimadzu GC 2010) equipped with a DB-35 60 m×0.32 mm capillary column and a flame ionization detector (FID). And the products were qualitatively analyzed by using gas chromatography~mass spectrometry (Shimadzu GC~MS 2010). The catalytic activity of the catalysts was obtained by calculating the rate of benzene hydrogenation (r) according to the following equation:

$$r = n_{conversion\ of\ benzene} / (n_{total\ ruthenium} \times t)$$

where $n_{conversion\ of\ benzene}$, t and $n_{total\ ruthenium}$ represent mols of conversing benzene, reaction time (h) and total mols of ruthenium in the catalysts. The unit of r is mol mol_{Ru}^{-1} h^{-1}.

View Article Online
DOI: 10.1039/C7CE00702G

3 Results and discussion

3.1 Influence of hydrothermal temperature on morphology of CoNi

XRD patterns for the as-synthesized CoNi structures under different hydrothermal temperatures (120 °C, 150 °C or 180 °C) are shown in Fig. 1. The peaks at 2θ = 44.4°, 51.7° and 76.1° can be attributed to CoNi(111), CoNi(200) and CoNi(220) planes of the face-centered cubic (fcc) phase of the CoNi alloy.[30] It indicates that the CoNi alloy materials have formed. And the peak with quite low intensity located at 2θ = 47.6° is ascribed to Co(101) plane of hexagonal close packed (hcp) cobalt (JCPDS card No. 05-0727). The standard peaks of fcc cobalt are described below: Co(111)-44.2°, Co(200)-51.5° and Co(220)-75.9° (JCPDS card No. 15-0806). The standard peaks of fcc nickel are described below: Ni(111)-44.5°, Ni(200)-51.8° and Co(220)-76.4° (JCPDS card No. 04-0850). Although ruthenium is supported on the CoNi crystal, there is no any diffraction peak corresponding to reduced or oxidized state ruthenium crystallite phase. It suggests that ruthenium maybe in the form of single atoms or nanoclusters is well dispersed. And XRD patterns of the CoNi-120-ethanol and the corresponding Ru/CoNi-120-ethanol catalyst are very similar to those of the CoNi-X samples and Ru/CoNi-X catalysts (figure not given). Based on the XRD results, it can be inferred that the CoNi alloy formed when the ratio of Ni to Co was 1:1.

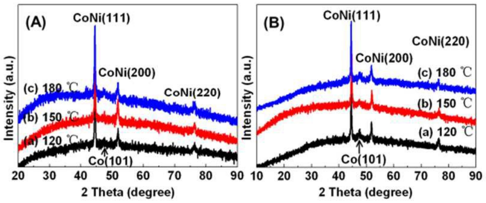

Fig. 1. (A) Powder XRD patterns for the CoNi crystals synthesized at different temperatures: (a) 120 °C, (b) 150 °C and (c) 180 °C; (B) Powder XRD patterns for the Ru/CoNi catalysts: (a) Ru/CoNi-120, (b) Ru/CoNi-150 and (c) Ru/CoNi-180.

Fig. 2 shows the SEM images of the CoNi materials synthesized at different hydrothermal temperatures (Fig. 2a-d~120 °C, Fig. 2e-h~150 °C and Fig. 2i-l~180 °C). As shown in Fig. 2a-h, the flower-like CoNi alloy structure with the size of 2~6 μm can be clearly seen. And some flower-like CoNi crystals stick together. The flower-like CoNi consists of a flower core and some petals. Most petals in the CoNi-120 sample look like flat leaves, but in the CoNi-150 sample they begin to grow column-like. The formation of this flower-like CoNi probably goes through two steps: the first step is the producing of the flower core, and the second step is the growing of petals. The morphologies of the crystals depend on the nucleation and growth rate to some extent. Our previous works reported that the Ni(111) planes grow preferably, due to the high surface energy of different planes in the order of (111) > (100) > (110).[46] Herein, the growing regularity of CoNi alloy is similar to that of monometallic Ni crystal. So with the hydrothermal temperature increasing to 150 °C, the petals would grow column-like. When the temperature successively increased up to 180 °C, the CoNi crystal became mushroom-like with the diameter of ~1 μm. The surface of each mushroom is circular, looking like the surface of a micro-sphere. The reason is that the growth rate of three different crystal planes is almost the same at such high temperature.[47]

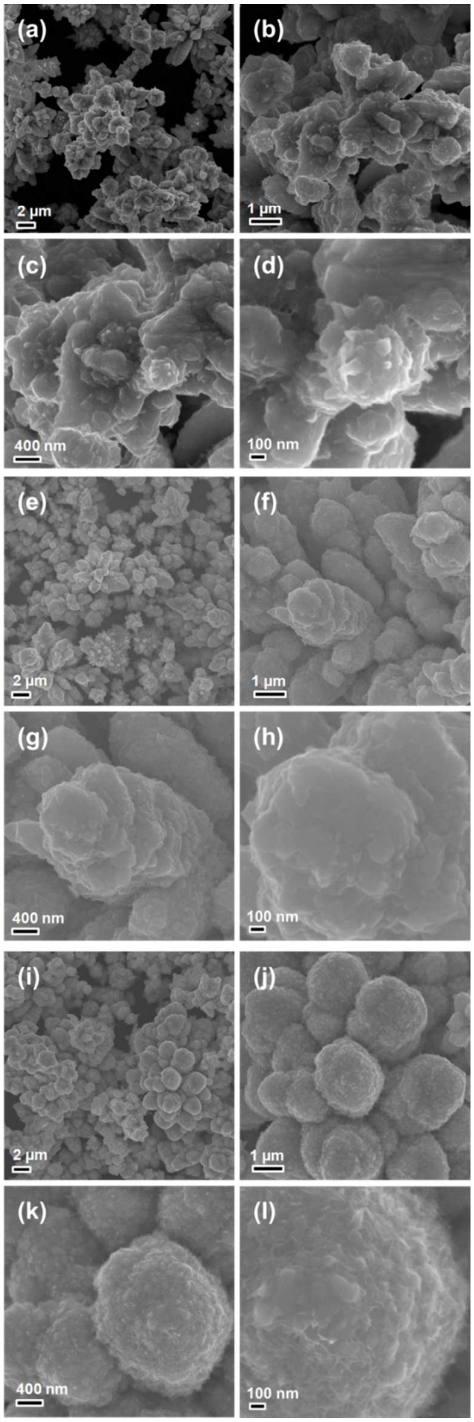

Fig. 2. SEM images of the CoNi crystal prepared at hydrothermal temperature of (a-d) 120 °C, (e-h) 150 °C and (i-l) 180 °C observed under different magnifications.

View Article Online
DOI: 10.1039/C7CE00702G

SEM images of the Ru/CoNi-120 catalyst are given in Fig. 3. Although ruthenium was loaded on the surface of the CoNi-120 sample, its structure and morphology were without any change. It suggests that the structure of flower-like CoNi is very stable. Therefore, a conclusion can be drawn that the morphology of CoNi crystal remains unchanged despite a small quantity of ruthenium atoms on it.

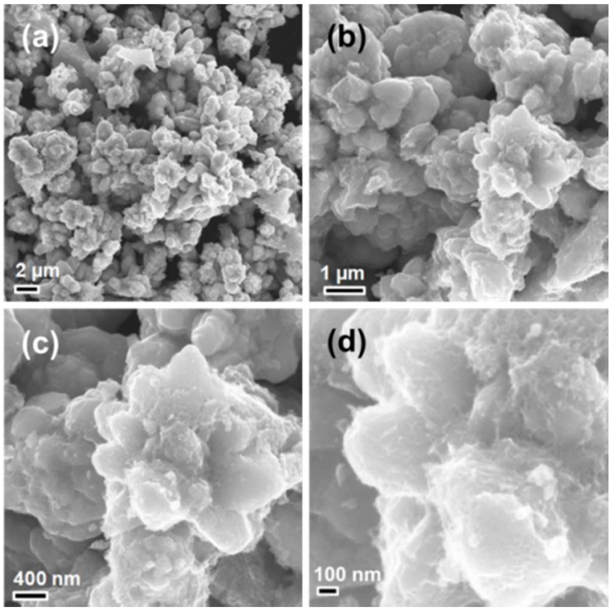

Fig. 3. SEM images of the Ru/CoNi-120 catalyst observed under different magnifications.

SEM-EDS analysis results of CoNi-120, CoNi-150, CoNi-180 and Ru/CoNi-120 samples are provided in Fig. 4. According to the EDS spectrum, oxygen, nickel and cobalt are detected in the selected black spot region in the image, including the contaminated carbon. It demonstrates that one CoNi crystal unit consists of Ni and Co element, implying the production of CoNi bimetallic particles. Combined with the above XRD characterization results, it is certain that the CoNi alloy structure has formed and the Ni/Co ratio is close to the added theoretical Ni^{2+}/Co^{2+} ratio-1:1. EDS spectra of the Ru/CoNi-120 catalyst proves that ruthenium has been successfully supported on the CoNi crystal. And the Ru loading is 1.10 wt%, in good agreement with ICP-MS analysis results.

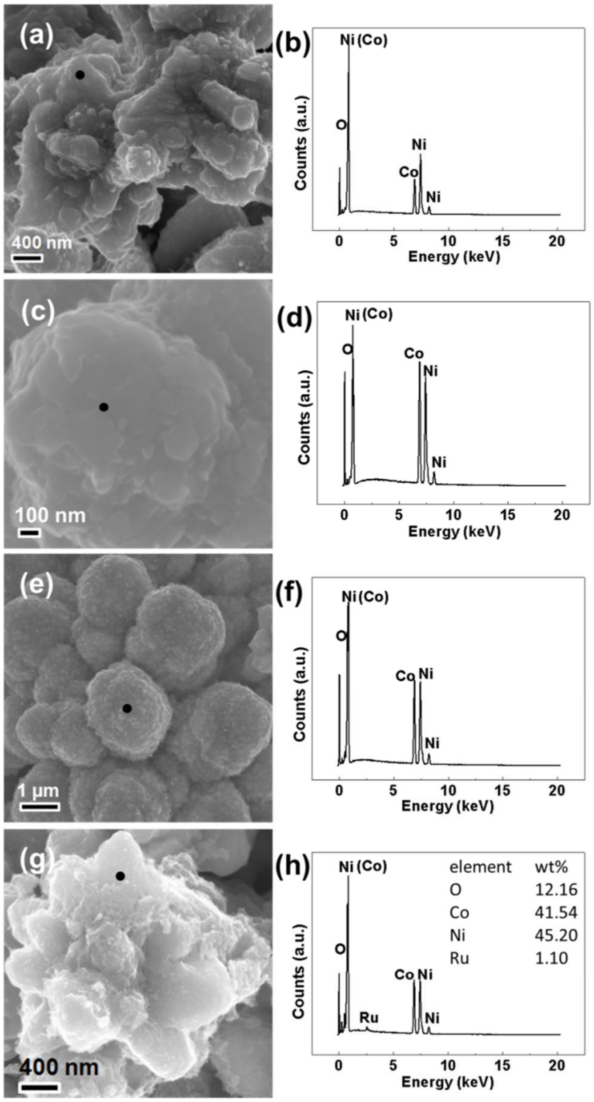

Fig. 4. SEM images of the CoNi crystal prepared at hydrothermal temperature of (a) 120 °C, (c) 150 °C, (e) 180 °C and (g) Ru/CoNi-120; EDS spectrums for the selected black spot region in (b) image a. (d) image c, (f) image e and (h) image g.

3.2 Influence of solvent on morphology of CoNi

Fig. 5 shows the XRD patterns of the CoNi crystal prepared by using ethanol as solvent, with other synthesis conditions identical with those of preparing above CoNi-120. It is revealed that the diffraction peaks are also with the CoNi alloy characteristic, indicating the successful preparation of CoNi alloy structure.

View Article Online
DOI: 10.1039/C7CE00702G

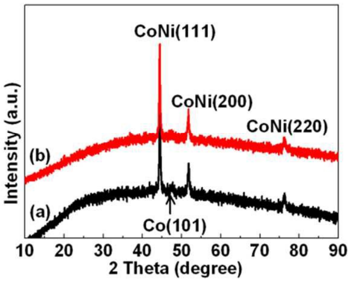

Fig. 5. Powder XRD patterns for (a) CoNi synthesized with ethanol as solvent (CoNi-120-ethanol) and (b) corresponding Ru/CoNi catalyst (Ru/CoNi-120-ethanol). Other synthesis conditions: hydrothermal temperature, 120 °C; hydrothermal time, 1 h; EDA, 5 mL; hydrazine hydrate, 5 mL.

To investigate the effect of solvent on the shape of CoNi crystal, the ethanol mixture of $NiCl_2$ (0.6500 g) and $CoCl_2$ (0.6500 g) solution substituted for the aqueous mixture of $NiCl_2·6H_2O$ and $CoCl_2·6H_2O$ solution while other synthesis parameters remained unchanged (hydrothermal time 1 h, hydrothermal temperature 120 °C, EDA, 5 mL, NaOH 1.8130 g, hydrazine hydrate 5 mL). The images of the as-obtained CoNi-120-ethanol sample are shown in Fig. 6. All of the CoNi crystals are with uniform dendrite-like shape in micrometer scale. Each dendrite is composed of many small sub-branches in nanometer scale, trunks and branches, which possess much more defect sites. It is probably beneficial for the improvement of its catalytic performance. The large difference in the morphology between the CoNi-120 and CoNi-120-ethanol samples may be attributable to different solvents, because the dielectric constant is different for various solvents, resulting in distinct surface energy of newly generated cobalt-nickel.[47,48] Based on the above results, a conclusion that the morphology of CoNi remained after a small amount of Ru supported on it has been obtained, so the shape of Ru/CoNi-120-ethanol is identical to CoNi-120-ethanol.

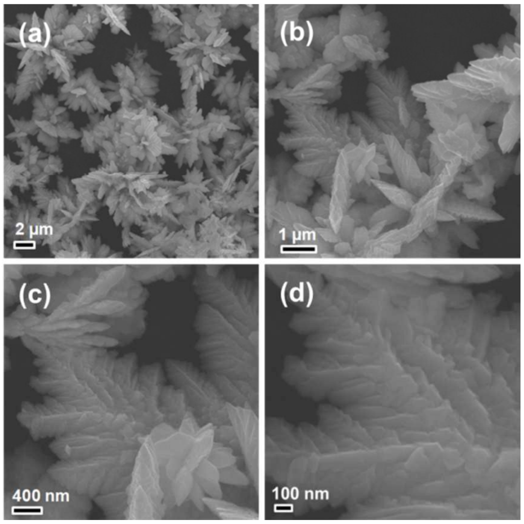

Fig. 6. SEM images of the CoNi crystal (CoNi-120-ethanol) prepared by using ethanol as solvent observed under different magnifications.

According to the above analysis results, a growth mechanism of different shapes of CoNi alloy crystal is proposed in Fig. 7. As depicted, firstly, the $[Ni(EDA)_2]^{2+}$ and $[Co(EDA)_2]^{2+}$ complexes are reduced by hydrazine hydrate, forming the CoNi alloy nanospheres. Secondly, the produced CoNi alloy nanoparticles serve as a center, which provide new nucleation sites favorable for continuous nucleation and growth of cobalt-nickel nanocrystals with anisotropic morphologies.[30,49,50] And due to the magnetic property of CoNi particles, the magnetic field strength at both ends of the pole magnet is larger than at other positions.[51] And the CoNi nuclei forming during later synthesis process tend to be attracted by the protruding parts of the core via the magnetic dipole interactions and added to the tip of protruding parts. As the growth proceeds, more and more petals will be produced on the surface of the cores, finally forming flower-like CoNi crystal. The probable growth mechanism given in this investigation is similar to that of the flower-like nickel and cobalt structure.[49,52-55] Therefore, the flower-like CoNi alloy structure form at relatively low temperature of 120 °C by hydrothermal approach. But with the hydrothermal temperature increasing to 150 °C or 180 °C, the flower-like morphology is transformed into the shape of column-like or mushroom-like, respectively. The reason is that high temperature increases the nucleation and growth rates of crystal, resulting in more nucleuses and growth in each orientation. It is beneficial to generate the CoNi structures with smooth surface, such as column-like or mushroom-like CoNi (containing CoNi nanospheres). Interestingly, the dendrite-like CoNi alloy microstructure appears when the synthesis process of CoNi is performed with ethanol as solvent. This is because the dielectric constant of ethanol is distinct from that of water, resulting in different solubility of Ni^{2+} and Co^{2+} ions in the solvent, as well as the rates of nucleation and growth of CoNi.

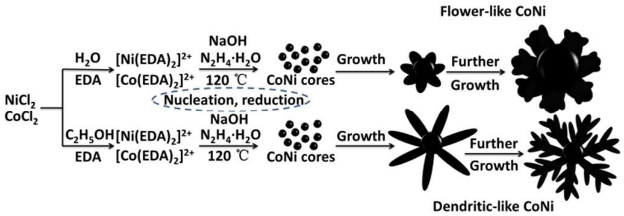

Fig. 7. Schematic illustration of the possible formation mechanism for the flower-like and dendrite-like CoNi alloy microstructure.

3.3 XPS characterization for the Ru/CoNi catalysts

With the purpose of obtaining the chemical state and general element composition on the surface of the catalysts, XPS analysis was performed on the typical catalysts (Ru/CoNi-120-ethanol and Ru/CoNi-150) and the results are shown in Fig. 8. In the Ni 2p XPS spectra of these two catalysts (Fig. 8A,B), the four doublets peaks located at the binding energies of 852.7 eV and 870 eV, 853.9 eV and 871.2 eV, 855.4 eV and 872.9 eV, 857.1 eV and 874.4 eV, can be ascribed to related Ni species in Ni(0), NiO, $Ni(OH)_2$ and NiOOH, respectively. The other two peaks with the binding energies of 861.6 eV and 879.7 eV may be assigned to shake-up satellite.[56,57] By calculating the peak area corresponding to different species, it can be obviously found that the oxidation state nickel (such as nickel oxide, nickel hydroxide and hydroxy nickel oxide) is predominant. The abundant existence of oxidized state nickel is mainly due to Ni(0) atoms on the surface easily oxidized in air and moisture environment prior to XPS tests.[32] In the Co 2p XPS spectra (Fig. 8C,D), the peaks centered at the binding energies of 778.2 eV (793.4 eV), 780.2 eV (795.4 eV) and 781.1 eV (796.3 eV) correspond to Co(0), CoO and

View Article Online
DOI: 10.1039/C7CE00702G

$Co(OH)_2$ species, also with two 'shake-up' peaks.[58,59] The surface composition of oxidized state cobalt is much higher than Co(0). By comparing the peak area corresponding to each specie in the Ni 2p XPS spectra of these two catalysts, it can be deduced that Ni(0) atoms on the surface of Ru/CoNi-120-ethanol are more easily oxidized than those on the surface of Ru/CoNi-150. Similar conclusion can be made based on the Co 2p XPS spectra. This is probably because nickel and cobalt atoms on the edges of the branches of dendrite-like CoNi, due to their lower coordination number, are more active than those on the surface of column-like CoNi.

The XPS signals in Fig. 8E,F are the Ru 3p XPS spectra of the Ru/CoNi-120-ethanol and Ru/CoNi-150 catalysts. The peaks at the binding energy values of 462 eV and 484 eV are attributed to Ru(0), while 464.2 eV and 486.2 eV are related to Ru^{4+} in the form of RuO_2.[60,61] It can be obviously found that the ratio of surface Ru^{4+} to Ru(0) of the Ru/CoNi-120-ethanol catalyst is slightly higher than that of the Ru/CoNi-150 catalyst, maybe owing to higher Ru dispersion on CoNi for the Ru/CoNi-120-ethanol catalyst, which is more easily oxidized in air.

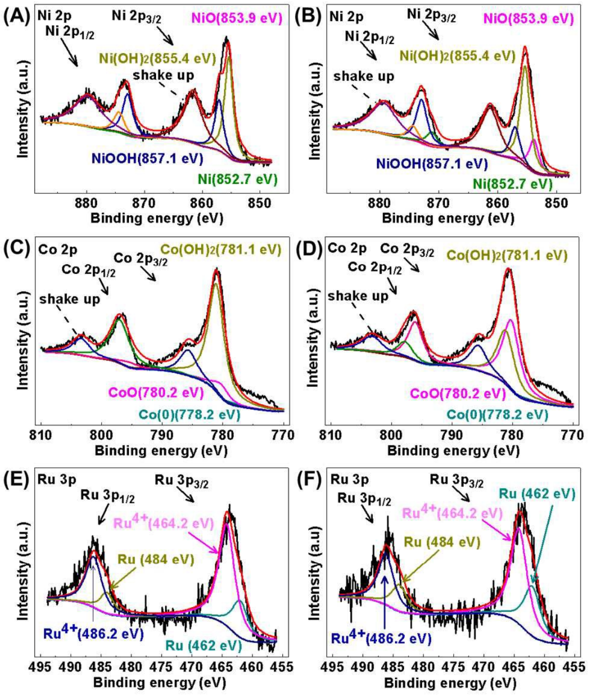

Fig. 8. Ni 2p XPS spectra of (A) Ru/CoNi-120-ethanol and (B) Ru/CoNi-150; Co 2p XPS spectra of (C) Ru/CoNi-120-ethanol and (D) Ru/CoNi-150; and Ru 3p XPS spectra of (E) Ru/CoNi-120-ethanol and (F) Ru/CoNi-150.

3.4 HS-LEIS results of the Ru/CoNi catalysts

The high-sensitivity low-energy ion scattering (HS-LEIS) technique has been considered as a powerful method for providing the atomic composition of the outmost surface.[62] HS-LEIS measurements for the catalysts were carried out to further confirm their different Ru dispersion and to obtain the atomic composition. The 3 keV $^4He^+$ HS-LEIS spectra for the Ru/CoNi-120-ethanol and Ru/CoNi-150 samples is displayed in Fig. 9A, which reveals that oxygen, nickel, cobalt and ruthenium co-exist on the outer surface of the catalysts. Another obvious characteristic is that the ratio of Ru atoms signal intensity/Ni(Co) atoms signal intensity in Ru/CoNi-120-ethanol is higher than that in Ru/CoNi-150. And we can come to the same conclusion from the 5 keV $^{20}Ne^+$ HS-LEIS spectra for these two catalysts (Fig. 9B). Therefore, on the basis of the same Ru loading in the Ru/CoNi catalysts, the HS-LEIS results indicate that Ru atoms are supported on CoNi with better dispersion in Ru/CoNi-120-ethanol than Ru/CoNi-150.

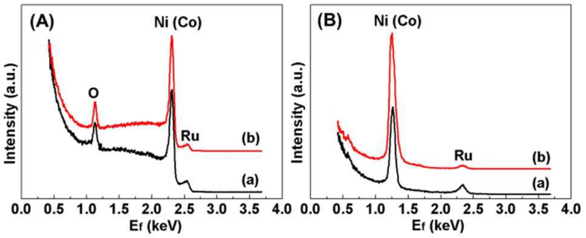

Fig. 9. (A) 3 keV $^4He^+$ and (B) 5 keV $^{20}Ne^+$ HS-LEIS spectra for (a) Ru/CoNi-120-ethanol and (b) Ru/CoNi-150.

3.5 Catalytic performance of the catalysts for benzene hydrogenation

The Ru/CoNi and CoNi-120-ethanol samples described above were applied in benzene hydrogenation. And the reaction results are listed in Table 1. Benzene was hardly converted to any product within 1 hour reaction time at 100 °C under the hydrogen pressure of 5.3 MPa (Table 1, Entry 1). For the Ru/CoNi-120 catalyst (flower-like) (Table 1, Entry 2), benzene conversion was 65% and the selectivity to cyclohexane was 100%, with a r of 13474.1 mol mol_{Ru}^{-1} h^{-1}. The yield to cyclohexane and r decreased when the hydrothermal synthesis temperature of CoNi increased to 150 °C (column-like) and 180 °C (mushroom-like) (Ru/CoNi-150~yield = 22% and r = 4560.4 mol mol_{Ru}^{-1} h^{-1}, Ru/CoNi-180~yield = 55% and r = 11400.8 mol mol_{Ru}^{-1} h^{-1}). The Ru/CoNi-120-ethanol catalyst (dendrite-like) gave the highest product yield~81% within the reaction time of 1 h. With the reaction time increasing up to 1.5 h, benzene was totally converted to cyclohexane. The most excellent catalytic activity of the Ru/CoNi-120-ethanol catalyst is mainly due to the high Ru dispersion and the synergistic effects of Ru, Ni and Co related species in the catalyst. And the accurate mechanism of this synergy effect will be illustrated in details later in our group.

Table 1. Catalytic performance of different catalysts for benzene hydrogenation.[a]

Entry	Catalyst (0.05 g)	Yield[b]	r (mol mol_{Ru}^{-1} h^{-1})
1	CoNi-120-ethanol	-	-
2	Ru/CoNi-120	65%	13474.1
3	Ru/CoNi-150	22%	4560.4
4	Ru/CoNi-180	55%	11400.8
5	Ru/CoNi-120-ethanol	81%	16791.0
6[c]	Ru/CoNi-120-ethanol	100%	13819.8

[a] Reaction conditions: benzene (10 mL), reaction time (1 h), reaction temperature (100 °C), reaction pressure (5.3 MPa) ; [b] Yield to cyclohexane; [c] reaction time (1.5 h).

View Article Online
DOI: 10.1039/C7CE00702G

Additionally, the Ru/CoNi-120-ethanol catalyst exhibited relatively high catalytic activity compared to most of the reported catalysts under similar reaction conditions.[32-34,44,61,63-66] For example, it showed much better catalytic performance than the monolithic Ni@Pd catalyst for benzene hydrogenation under milder reaction conditions.[44] And the stability of the Ru/CoNi-120-ethanol catalyst in benzene hydrogenation reaction is shown in Fig. 10A. The results demonstrate that there is no obvious deactivation of the catalyst after recycled for five times. SEM measurement for the recycled Ru/CoNi-120-ethanol catalyst was also performed, and SEM image is displayed in Fig. 10B. The dendrite-like crystals can be clearly seen. The morphology of the catalyst was without change before and after catalytic reaction. Therefore, we can infer that the Ru/CoNi catalysts are relatively stable during reaction.

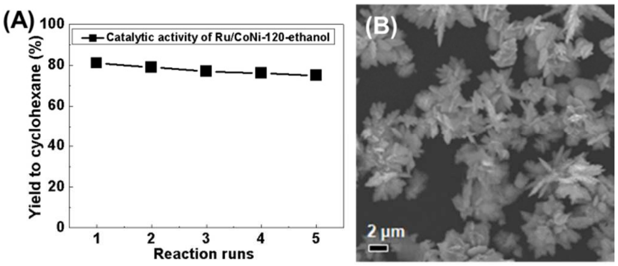

Fig. 10. (A) Stability of the Ru/CoNi-120-ethanol catalyst for benzene hydrogenation, reaction conditions: benzene (10 mL), reaction time (1 h), reaction temperature (100 °C), reaction pressure (5.3 MPa); and (B) SEM image of the Ru/CoNi-120-ethanol catalyst recycled for five runs.

4 Conclusions

In conclusion, the CoNi alloy crystal with the flower-like and mushroom-like shape was synthesized by modulating the hydrothermal synthesis temperature with water as solvent. And the dendrite-like CoNi nanomaterial was obtained at 120 °C by using ethanol as solvent. We have explained the probable formation mechanism for the flower-like and dendrite-like CoNi alloy crystal. The corresponding Ru/CoNi catalysts (Ru-on-CoNi alloy crystal) were synthesized by galvanic replacement reaction and applied in benzene hydrogenation reaction. The Ru/CoNi-120-ethanol catalyst with the morphology of dendrite-like exhibited the best catalytic performance among the as-obtained Ru/CoNi catalysts with different shapes in this work, with 100% yield to cyclohexane and *r* of 13819 mol mol_{Ru}^{-1} h^{-1} under the reaction conditions of reaction time (1.5 h), reaction temperature (100 °C) and reaction pressure (5.3 MPa H_2). The excellent catalytic property of the Ru/CoNi-120-ethanol catalyst with dendrite-like shape is probably due to the high Ru dispersion, numerous defect sites and positive synergistic effect among ruthenium, nickel and cobalt related species.

Acknowledgements

The works reported in this publication were funded by the Natural Science Foundation of Jiangxi Province of China (Grant No. 20161BAB213083), Research Foundation of Education Bureau of Jiangxi Province of China (GJJ160666), Doctor Starting Foundation of Jiangxi University of Science and Technology of China (Grant No. jxxjbs15008), and National Natural Science Foundation of China (Grant No. 21466013).

Notes and references

1 D. M. Alonso, S. G. Wettstein and J. A. Dumesic, *Chem. Soc. Rev.*, 2012, **41**, 8075–8098.
2 L. Kesavan, R. Tiruvalam, M. H. Ab Rahim, M. I. bin Saiman, D. I. Enache, R. L. Jenkins, N. Dimitratos, J. A. Lopez-Sanchez, S. H. Taylor, D. W. Knight, C. J. Kiely and G. J. Hutchings, *Science*, 2011, **331**, 195–199.
3 S. Wang, Z. Xin, X. Huang, W. Yu, S. Niu and L. Shao, *Phys. Chem. Chem. Phys.*, 2017, **19**, 6164–6168.
4 C. K. S. Choong, L. Chen, Y. Du, M. Schreyer, S. W. D. Ong, C. K. Poh, L. Hong and A. Borgna, *Phys. Chem. Chem. Phys.*, 2017, **19**, 4199–4207.
5 N. M. AlYami, A. P. LaGrow, K. S. Joya, J. Hwang, K. Katsiev, D. H. Anjum, Y. Losovyj, L. Sinatra, J. Y. Kim and O. M. Bakr, *Phys. Chem. Chem. Phys.*, 2016, **18**, 16169–16178.
6 J. Y. Park, Y. Zhang, S. H. Joo, Y. Jung and G. A. Somorjai, *Catal. Today*, 2012, **181**, 133–137.
7 C.-Y. Lu, H.-H. Tseng, M.-Y. Wey, L.-Y. Liu and K.-H. Chuang, *Mater. Sci. Eng. B*, 2009, **157**, 105–112.
8 S. Alayoglu, A. U. Nilekar, M. Mavrikakis and B. Eichhorn, *Nat. Mater.*, 2008, **7**, 333–338.
9 X. Liu, D. Wang and Y. Li, *Nano Today*, 2012, **7**, 448–466.
10 M. Y. Rafique, L. Pan, W. S. Khan, M. Z. Iqbal, H. Qiu, M. H. Farooq, M. Ellahi and Z. Guo, *CrystEngComm*, 2013, ***15***, 5314–5325.
11 H. Li, J. Liao, Y. Du, T. You, W. Liao and L. Wen, *Chem. Commun.*, 2013, ***49***, 1768–1770.
12 R. Ferrando, J. Jellinek and R. L. Johnston, *Chem. Rev.*, 2008, **108**, 845–810.
13 O. Ergeneman, K. M. Sivaraman, S. Pané, E. Pellicer, A. Teleki, A. M. Hirt, M. D. Baró and B. J. Nelson, *Electrochim. Acta*, 2011, **56**, 1399–1408.
14 B. M. Muñoz-Flores, B. I. Kharisov, V. M. Jiménez-Pérez, P. E. Martínez and S. T. López, *Ind. Eng. Chem. Res.*, 2011, **50**, 7705–7721.
15 L. Chen, Q. Zhu, Z. Hao, T. Zhang and Z. Xie, *Int. J. Hydrogen Energy*, 2010, **35**, 8494–8502.
16 Q. Y. Liu, X. H. Guo, T. J. Wang, Y. Li and W. J. Shen, *Mater. Lett.*, 2010, **64**, 1271–1274.
17 P. Cojocaru, L. Magagnin, E. Gomez, E. Vallés, F. Liu, C. Carraro and R. Maboudian, *J. Micromech. Microeng.*, 2010, **20**, 125017–125022.
18 R. Brayner, V. Marie-Josèphe, F. Fiévet and T. Coradin, *Chem. Mater.*, 2007, **19**, 1190–1198.
19 T. Yamauchi, Y. Tsukahara, K. Yamada, T. Sakata and Y. Wada, *Chem. Mater.*, 2011, **23**, 75–84.
20 X. Guo, L. I. Yong, Q. Liu and W. Shen, Chin. *J. Catal.*, 2012, **33**, 645–650.
21 M. J. Hu, B. Lin and S. H. Yu, *Nano Res.*, 2008, **1**, 303–313.
22 N. A. M. Barakat, K. A. Khalil, I. H. Mahmoud, M. A. Kanjwal, F. A. Sheikh and H. Y. Kim, *J. Phys. Chem. C*, 2010, **114**, 15589–15593.
23 A. Arief and P. K. Mukhopadhyay, *J. Magn. Magn. Mater.*, 2014, **372**, 214–223
24 L. Dong, Y. Liu, Y. Lu, L. Zhang, N. Man, L. Cao, K. Ma, D. An, J. Lin, Y. J. Xu, W. P. Xu, W. B. Wu and S. H. Yu, *Adv. Funct. Mater.*, 2013, **23**, 5930–5940.
25 M. H. Rashid, M. Raula and T. K. Mandal, *J. Mater. Chem.*, 2011, **21**, 4904–4917.
26 M.-J. Hu, Y. Lu, S. Zhang, S.-R. Guo, B. Lin, M. Zhang and S.-H. Yu, *J. Am. Chem. Soc.*, 2008, **130**, 11606–1167.
27 D.-E. Zhang, X.-M. Ni, X.-J. Zhang and H.-G. Zheng, *J. Magn. Magn. Mater.*, 2006, **302**, 290–293.

View Article Online
DOI: 10.1039/C7CE00702G

28 D. Ung, Y. Soumare, N. Chakroune, G. Viau, M.-J. Vaulay, V. Richard and F. Fiévet, *Chem. Mater.*, 2007, **19**, 2084–2094.

29 M. Wen, Y.-F. Wang, F. Zhang and Q.-S. Wu, *J. Phys. Chem. C*, 2009, **113**, 5960–5966.

30 H. Li, J. Liao, Y. Feng, S. Yu, X. Zhang and J. Zhen, *CrystEngComm*, 2012, **14**, 2974–2980.

31 Z. An, J. Zhang and S. Pan, *CrystEngComm*, 2010, 12, 500–506.

32 Y. Sun, C. Li and A. Zhang, *Appl. Catal. A: Gen.*, 2016, **522**, 180–187.

33 F. Domínguez, J. Sánchez, G. Arteaga and E. Choren, *J. Mol. Catal. A: Chem.*, 2005, **228**, 319–324.

34 Y. Ma, Y. Huang, Y. Cheng, L. Wang and X. Li, *Appl. Catal. A: Gen.*, 2014, **484**, 154–160.

35 M. Zahmakıran, Y. Tonbul and S. Özkar, *J. Am. Chem. Soc.*, 2010, **132**, 6541–6549.

36 A. Horváth, A. Beck, Z. Koppány, A. Sárkány and L. Guczi, *J. Mol. Catal. A: Chem.*, 2002, **182–183**, 295–302.

37 A. Roucoux, J. Schulz and H. Patin, *Adv. Synth. Catal.*, 2003, **345**, 222–229.

38 Y. Tonbul, M. Zahmakiran and S. Özkar, *Appl. Catal. B: Environ.*, 2014, **148–149**, 466–472.

39 B. Yoon, H.-B. Pan and C. M. Wai, *J. Phys. Chem. C*, 2009, **113**, 1520–1525.

40 Y. Huang, Y. Ma, Y. Cheng, L. Wang and X. Li, *Ind. Eng. Chem. Res.*, 2014, **53**, 4604–4613.

41 Y. Huang, Y. Ma, Y. Cheng, L. Wang and X. Li, *Catal. Commun.*, 2015, **69**, 55–58.

42 K. D. Gilroy, S. D. Golze, A. Yaghoubzade, E. Menumerov, R. A. Hughes and S. Neretina, *ACS Nano*, 2016, **10**, 6354–6362.

43 S. F. Tan, G. Lin, M. Bosman, U. Mirsaidov and C. A. Nijhuis, *ACS Nano*, 2016, **10**, 7689–7695.

44 Y. Li, L. Zhu, K. Yan, J. Zheng, B. H. Chen and W. Wang, *Chem. Eng. J.*, 2013, **226**, 166–170.

45 L. Zhu, Y. Jiang, J. Zheng, N. Zhang, C. Yu, Y. Li, C.-W. Pao, J.-L. Chen, C. Jin, J.-F. Lee, C.-J. Zhong and B. H. Chen, *Small*, 2015, **11**, 4385–4393.

46 P. Li, N. Wang and R. Wang, *Eur. J. Inorg. Chem.*, 2010, 2261–2265.

47 C. Wang, X. Han, P. Xu, J. Wang, Y. Du, X. Wang, W. Qin and T. Zhan, *J. Phys. Chem. C*, 2010, **114**, 3196–3203.

48 D. P. Wang, D. B. Sun, H. Y. Yu and H. M. Meng, *J. Cryst. Growth*, 2008, **310**, 1195–1201.

49 Q. Liu, X. Guo, Y. Li and W. Shen, *J. Phys. Chem. C*, 2009, **113**, 3436–3441.

50 X.-M. Liu and S.-Y. Fu, J. Cryst. Growth, 2007, **306**, 428–432.

51 J. Ye, Q.-W. Chen, H.-P. Qi and N. Tao, *Cryst. Growth Des.*, 2008, **8**, 2464–2468.

52 R. H. Wang, J. S. Jiang and M. Hu, *Mater. Res. Bull.*, 2009, **44**, 1468–1473.

53 Y. Wang, Q. Zhu and H. Zhang, *Mater. Res. Bull.*, 2007, **42**, 1450–1456.

54 S. Senapati, S. K. Srivastava, S. B. Singh and K. Biswas, *Cryst. Growth Des.*, 2010, **10**, 4068–4075.

55 A. Mathew, N. Munichandraiah and G. M. Rao, *Mater. Sci. Eng. B*, 2009, **158**, 7–12.

56 P.-P. Li, W.-Z. Lang, K. Xia, L. Luan, X. Yan and Y.-J. Guo, *Appl. Catal. A: Gen.*, 2016, **522**, 172–179.

57 Q. Liu, D. Ding, C. Ning and X. Wang, *Mater. Sci. Eng. B*, 2015, **202**, 54–60.

58 L. Zhuo, J. Ge, L. Cao and B. Tang, *Cryst. Growth Des.*, 2009, **9**, 1–6.

59 L. Ma, L. Xu, X. Xu, X. Zhou, J. Luo and L. Zhang, *Mater. Sci. Eng. B*, 2016, **212**, 30–38.

60 Y. Yamauchi, T. Ohsuna and K. Kuroda, *Chem. Mater.*, 2007, **19**, 1335–1342.

61 S. Miao, Z. Liu, B. Han, J. Huang, Z. Sun, J. Zhang and T. Jiang, *Angew. Chem., Int. Ed.*, 2006, **45**, 266–269.

62 H. H. Brongersma, M. Draxler, M. de Ridder and P. Bauer, *Surf. Sci. Rep.*, 2007, **62**, 63–109.

63 F. Su, L. Lv, F. Y. Lee, T. Liu, A. I. Cooper and X. S. Zhao, *J. Am. Chem. Soc.*, 2007, **129**, 14213–14223.

64 K. X. Yao, X. Liu, Z. Li, C. C. Li, H. C. Zeng and Y. Han, *ChemCatChem*, 2012, **4**, 1938–1942.

65 P. Dyson, D. Ellis and D. Parker, *Chem. Commun.*, 1999, 25–26.

66 Y. Zhao, J. Zhang, J. Song, J. Li, J. Liu, T. Wu, P. Zhang and B. Han, *Green Chem.*, 2011, **13**, 2078–2082.